Endocyclic and Exocyclic Cleavage of Phosphorane Monoanion: A Detailed Mechanism of the RNase A Transphosphorylation Step[†,‡]

Carmay Lim* and Philip Tole

Contribution from the Department of Molecular and Medical Genetics, Department of Chemistry and Department of Biochemistry, University of Toronto, 1 King's College Circle, Toronto, Ontario M5S 1A8, Canada. *Received December 16, 1991*

Abstract: The free energy profile for $(HOC_2H_4PO_4CH_3)^- \rightarrow (C_2H_4PO_4)^- + MeOH$, modelling the transphosphorylation step in RNase A catalysis, is explored using ab initio molecular orbital calculations. Geometry optimizations are carried out at the Hartree-Fock level with the 3-21+G* basis set. The correlation energy is estimated with second-order Møller-Plesset theory and the 6-31+G* basis using fully optimized 3-21+G* geometries. The gas-phase reaction, $(HOC_2H_4PO_4CH_3)^- \rightarrow (C_2H_4PO_4)^- + MeOH$, is computed to proceed via a stepwise mechanism involving a monoanionic *pentacovalent* intermediate which has to rotate about an equatorial P-O(H) bond to yield a phosphorane monoanion in a conformation activated for exocyclic cleavage. The stereochemistry of the gas-phase reaction is in accord with an in-line mechanism. The pentacovalent intermediates and transition states have a distorted trigonal-bipyramidal geometry, and the conformation of the transition states are activated for endocyclic and exocyclic cleavage. A detailed mechanism of the RNase A-catalyzed transphosphorylation step is presented and compared to other proposed mechanisms as well as to the nonenzymatic reaction in solution.

1. Introduction

The enzyme ribonuclease A (RNase A) catalyzes the degradation of ribonucleic acid (RNA) in two steps,[1-3] transphosphorylation to form a 2',3'-cyclic phosphate intermediate and hydrolysis of the latter to yield a 3'-terminal phosphate group. According to the established mechanism,[1-3] a neutral His 12 and a protonated His 119 act as a general base and acid, respectively, in the first step and reverse their roles in the second step. Breslow and co-workers[4-6] have proposed a new mechanism for catalysis of RNA cleavage by RNase A based on kinetic studies of the reactions of polyuridylic acid [poly(U)] and the dinucleotides 3',5'-UpU and 3',5'-ApA. In their proposed mechanism, the transphosphorylation and hydrolysis steps occur in a sequential mechanism involving a pentacovalent phosphorane intermediate. In particular, their proposed transphosphorylation mechanism assumes two steps: in the first step, a positively charged His 119 protonates the phosphate and a neutral His 12 deprotonates the 2'-hydroxyl group to form a pentavalent phosphorane monoanion; in the second step, His 119 removes the proton on the phosphoryl oxygen and delivers it to the leaving oxygen to form a five-membered cyclic phosphate intermediate.

The requirement that His 12 deprotonates the 2'-hydroxyl group in the standard mechanism and that His 119 protonates the phosphate anion in Breslow's mechanism appears to be inconsistent with their pK_a values. In the former case, the pK_a of the 2'-hydroxyl group, estimated to be around 14 from the pK_a of a serine side chain,[7] is greater than that of His 12 (pK_a = 5.8-6.0);[8] in the latter case, the pK_a of a phosphate group, estimated to be around 1-3,[9] is smaller than that of His 119 (pK_a = 6.2-6.3).[8] In particular, the pK_a of His 119 in the RNase A/UpcA complex, 6.3,[10] is similar to its value in the free enzyme; it is expected to be more perturbed from its free enzyme value if His 119 were to fully protonate one of the phosphoryl oxygens. Proton NMR studies of the RNase A/UpcA complex[10] show that the phosphonyl group retains roughly two-thirds of its negative charge although some partial neutralizations may exist. Molecular dynamics simulations[11] of the RNase A/CpA complex with His 119 protonated and His 12 either neutral or positively charged show that when His 12 is neutral, atom NE2 hydrogen bonds to the sugar oxygen (O2'H), but when it is protonated, atom NE2 hydrogen bonds to a phosphoryl oxygen; atom ND1 of His 119, which is protonated in both simulations, hydrogen bonds to a phosphoryl oxygen. The experimental data and simulation results suggest an alternative mechanism for the first step of Breslow's proposed transphosphorylation; viz., His 119 hydrogen bonds, instead of giving up its proton, to a phosphoryl oxygen while His 12 facilitates the intramolecular transfer of the 2'-hydroxyl hydrogen to a phosphoryl oxygen (tautomeric conversion).

We have carried out quantum mechanical studies on model compounds to map out the RNase A transphosphorylation pathway; quantum mechanical calculations pertaining to the hydrolysis step have also been performed,[12] and some of the results have been reported.[13,14] We modelled the transphosphorylation step

$$\text{dinucleotide} \rightarrow \text{cyclic phosphate} + \text{alcohol} \qquad (1)$$

by:

$$\underset{\text{methyl hydroxyethyl phosphate (MHEP)}^-}{(HOC_2H_4PO_4CH_3)^-} \longrightarrow \underset{\text{ethylene phosphate (EP)}^-}{(C_2H_4PO_4)^-} + \underset{\text{methanol (MeOH)}}{CH_3OH} \qquad (2)$$

We modelled the above tautomeric conversion by ring-closure of methyl hydroxyethyl phosphate $(MHEP)^-$ where the reaction coordinate is defined by the O2'-H distance (Figure 1). A stable trigonal-bipyramidal monoanionic intermediate was found (Figure 2); this was used to model a phosphorane intermediate in reaction 1. We mapped out endocyclic and exocyclic cleavage of the phosphorane monoanion in Figure 2 (parts a and b, respectively) by choosing P-O2' and P-O5' as the reaction coordinate. The gas-phase profile for reaction 2 was calculated using ab initio

[†] This work was supported by the Protein Engineering Network Center of Excellence.

[‡] Keywords: tetrahedral phosphate and pentacovalent phosphorane intermediates/RNase A transphosphorylation.

(1) Richards, F. M.; Wyckoff, H. W. Bovine Pancreatic Ribonuclease. In *The Enzymes*; Academic Press: New York, 1971; Vol. 4, pp 647-806.
(2) Blackburn, P.; Moore, S. Pancreatic Ribonuclease. In *The Enzymes*; Academic Press: New York, 1982; Vol. 15, pp 317-433.
(3) Fersht, A. *Enzyme Structure and Mechanism*; W. H. Freeman: New York, 1985.
(4) Breslow, R.; Labelle, M. *J. Am. Chem. Soc.* **1986**, *108*, 2655-2659.
(5) Anslyn, E.; Breslow, R. *J. Am. Chem. Soc.* **1989**, *111*, 4473-4482.
(6) Breslow, R.; Huang, D.-L. *J. Am. Chem. Soc.* **1990**, *112*, 9621-9623.
(7) Metzler, D. E. *Biochemistry*; Academic Press: New York, 1977.
(8) Markley, J. L. *Biochemistry* **1975**, *14*, 3546-51.
(9) Emsley, J.; Hall, D. *The Chemistry of Phosphorus*; John Wiley and Sons: New York, 1976.
(10) Griffin, J. H.; Schechter, A. N.; Cohen, J. S. *Ann. N.Y. Acad. Sci.* **1973**, *222*, 693-708.
(11) Haydock, K.; Lim, C.; Brunger, A. T.; Karplus, M. *J. Am. Chem. Soc.* **1990**, *112*, 3826-3831.
(12) Lim, C.; Karplus, M., manuscript in preparation.
(13) Lim, C.; Karplus, M. *J. Am. Chem. Soc.* **1990**, *112*, 5872-5873.
(14) Dejaegere, A.; Lim, C.; Karplus, M. *J. Am. Chem. Soc.* **1991**, *113*, 4353-4355.

0002-7863/92/1514-7245$03.00/0

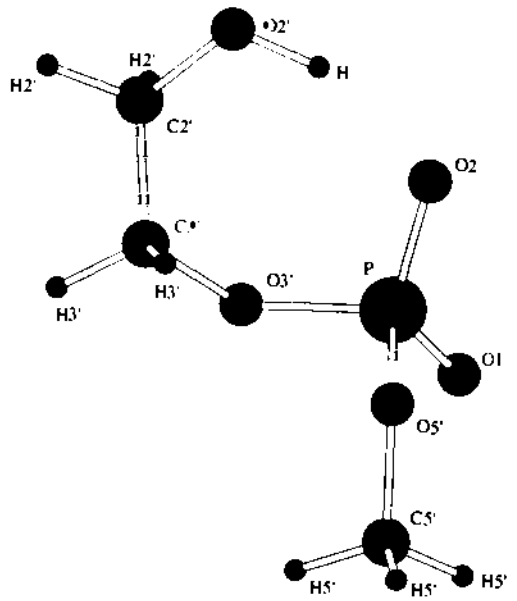

Figure 1. HF/3-21+G* fully optimized methyl 2'-hydroxyethyl phosphate $(MHEP)^-$; reaction coordinate for ring-closure of $(MHEP)^-$ is the O2'-H distance.

molecular orbital methods and the 3-21+G* basis with polarization functions (3d-orbitals) on the phosphorus and diffuse functions (s and p orbitals) added to the heavy atoms. Most of the calculations were made in the Hartree–Fock (HF) approximation, though we have estimated the importance of correlation effects by second-order Møller–Plesset perturbation theory (MP2) with a 6-31+G* basis set. In section 2, we briefly outline the method used for the quantum mechanical calculations. In section 3, we describe the results of the gas phase profile for the model reaction 2. The latter is compared to ab initio gas-phase reaction profiles involving dianionic intermediates[13-15] and its relevance to the RNase A-catalyzed transphosphorylation is discussed in section 4. We summarize our results in section 5.

2. Method

The ab initio calculations were performed using the program GAUSSIAN 90.[16] The 3-21+G* basis set was chosen since it is well-known that d-type orbitals on the second row elements are required to give a good description of hypervalent molecules such as pentavalent phosphorus and that addition of diffuse functions lowers energies of anions more than neutral molecules and provide a better description of their relative energies.[11] The 3-21+G* basis set yields geometries of cyclic and acyclic phosphate molecules which are in good agreement with experiment.[12,18,19] For example, comparison of the 3-21+G* structure of methyl ethylene phosphate[12] with the X-ray structure[18] shows that nearly all the bond lengths are within ±0.02 Å and most of the bond angles are within ±2° of experiment; the 3-21+G* structure of the dianion, $(HOC_3H_4PO_4)^{2-}$,[12] has three nearly equivalent P–O bonds, 1.514, 1.524, and 1.548 Å, in close agreement with 1.510, 1.514, and 1.519 Å, the mean values for 22 available alkyl phosphate dianion structures.[19] All geometries were fully optimized, unless stated otherwise. The electronic correlation energy was estimated by second-order Møller–Plesset perturbation theory (MP2). Since

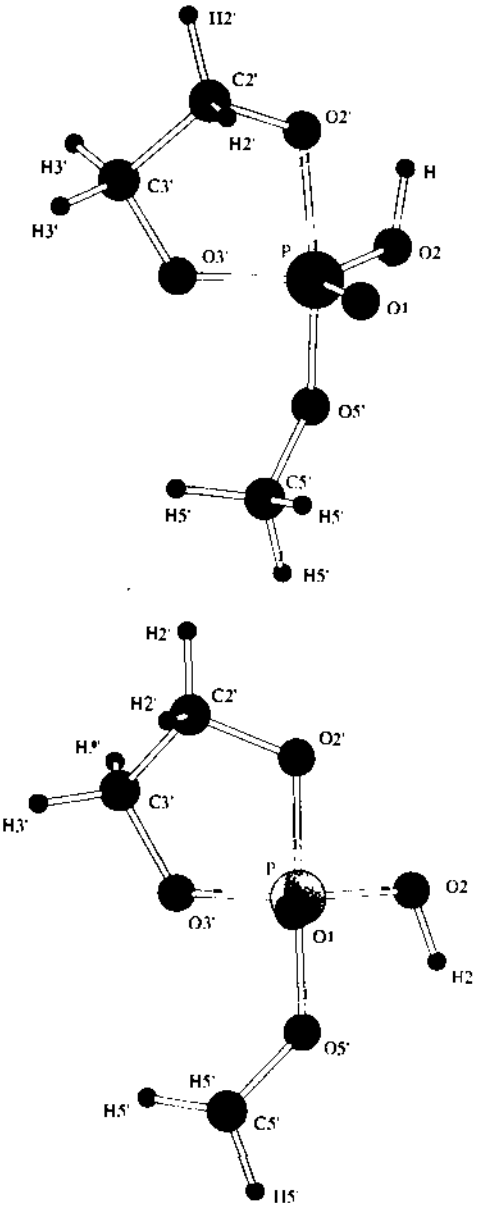

Figure 2. (a) HF/3-21+G* fully optimized $(L_GN)^-$ intermediate; reaction coordinate for endocyclic cleavage is the P–O2' distance. (b) HF/3-21+G* fully optimized $(L_GX)^-$ intermediate; reaction coordinate for exocyclic cleavage is the P–O5' distance.

a small basis set like 3-21+G* may limit the fraction of the total correlation energy obtainable, a larger 6-31+G* basis was employed. The MP2/6-31+G* computations were carried out for single points only corresponding to the 3-21+G* optimized geometries of the reactants, transition states, intermediates, and products of reaction 2. The results for $(EP)^-$ were taken from previous calculations.[12]

To determine the thermodynamic parameters, vibrational frequencies were computed for the fully optimized structures of the stationary points on the potential energy surface of reaction 2. The entropy (S_{vib}) and vibrational energy (E_{vib}) were calculated from the frequencies and geometries according to standard statistical mechanical formulas.[11] The rotational (E_{rot}) and translational (E_{trans}) energy and the work term (PV) were treated classically. Thus, the entropy change between two states is given by

$$\Delta S = \Delta S_{trans} + \Delta S_{rot} + \Delta S_{vib} \quad (3.1)$$

and the enthalpy change is given by

$$\Delta H = \Delta E + \Delta E_{trans} + \Delta E_{rot} + \Delta E_{vib} + P\Delta V \quad (3.2)$$

(15) Uchimaru, T.; Tanabe, K.; Nishikawa, S.; Taira, K. *J. Am. Chem. Soc.* **1991**, *113*, 4351–4353.
(16) Frisch, M. J.; Head-Gordon, M.; Trucks, G. W.; Foresman, J. B.; Schlegel, H. B.; Raghavachari, K.; Robb, M.; Binkley, J. S.; Gonzalez, C.; DeFrees, D. J.; Fox, D. J.; Whiteside, R. A.; Seeger, R.; Melius, C. F.; Baker, J.; Martin, R. L.; Kahn, L. R.; Stewart, J. J. P.; Topiol, S.; Pople, J. A. In *Gaussian 90*; Gaussian Inc.: Pittsburgh, PA, 15213, U.S.A.
(17) Hehre, W. J.; Radom, L.; Schleyer, P. v. R.; Pople, J. A. *Ab Initio Molecular Orbital Theory*; John Wiley and Sons: 1986.
(18) Chiu, Y. H.; Lipscomb, W. N. *J. Am. Chem. Soc.* **1969**, *91*, 4150–4155.
(19) Jones, P. G.; Sheldrick, G. M. *Acta Crystallogr.* **1984**, *C40*, 547–549.

Table I. 3-21+G* Total Energies (au) and Relative Energies (kcal/mol) as a Function of the Reaction Coordinate

reaction coordinate (Å)	HF/3-21+G* energies total (au)	HF/3-21+G* energies relative (kcal/mol)	MP2/6-31+G* energies[a] total (au)	MP2/6-31+G* energies[a] relative (kcal/mol)
Proton Transfer from O2′ to O2 in $(MHEP)^-$: Reaction Coordinate is O2′–H				
0.99[b]	−829.266 26	0.0	−834.875 75	0.0
1.10[c]	−829.260 00	3.9		
1.30[c]	−829.242 87	14.7		
1.50[c]	−829.226 72	24.8		
1.70[c]	−829.223 13	27.1		
1.96[d,e]	−829.215 47	31.9	−834.823 01	33.1
3.98[f]	−829.186 22	50.2	−834.794 23	51.2
Endocyclic Cleavage of $(I_{-G}N)^-$: Reaction Coordinate is P~O2′				
1.818[g]	−829.211 32	0.00	−834.828 43	0.0
2.018[d]	−829.208 08	2.04		
2.200[d]	−829.205 10	3.90		
2.292[h]	−829.204 69	4.16	−834.819 19	5.8
2.325[d]	−829.204 75	4.13		
2.350[d]	−829.204 86	4.06		
2.400[d]	−829.205 00	3.97		
3.545[b]	−829.266 26	−34.37	−834.875 75	−29.7
Exocyclic Cleavage of $(I_{-G}X)^-$: Reaction Coordinate is P~O5′				
1.726[i]	−829.211 07	0.0	−834.828 66	0.0
1.900[d]	−829.204 60	4.1		
2.100[d]	−829.191 98	12.0		
2.200[d]	−829.186 96	15.1		
2.313[j]	−829.183 61	17.2	−834.806 79	13.7
2.400[d]	−829.212 49	−0.89		
∞[k]	−829.222 77	−7.34	−834.840 28	−7.3

[a] Single point calculation at HF/3-21+G* geometry. [b] $(MHEP)^-$ reactant. [c] Stationary point from optimization of ring only. [d] Stationary point for fixed reaction coordinate. [e] $(MHEP)^-$ for fixed H–O2′ = 1.96 Å. [f] $(MEHP_T)^-$ tetrahedral intermediate. [g] $(I_{-G}N)^-$ pentacovalent intermediate. [h] $(TS_{-G}N)^-$ transition state. [i] $(I_{-G}X)^-$ pentacovalent intermediate. [j] $(TS_{-AC}X)^-$ transition state. [k] $(EP)^-$ + MeOH products.

where ΔE is the electronic energy change including electron correlation corrections and $PV = RT = 0.592$ kcal/mol. The entropy and enthalpy changes are combined to give the free energy.

Each of the monoanion structures except $(EP)^-$ has 45 degrees of freedom with 143 and 191 basis functions in the 3-21+G* and 6-31+G* basis sets, respectively. Using the program GAUSSIAN 90, an optimization cycle (1 SCF cycle) at the HF/3-21+G* level took about 2 h on a Stardent PS3030 with a memory requirement around 1.9 Megawords. A single point energy calculation at the MP2/6-31+G*//HF/3-21+G* level took about 36 min on a Cray XMP, and calculation of HF/3-21+G* frequencies took an average of 1 h 38 min Cray XMP CPU.

3. Results

Table I lists the total energies in atomic units (au) and relative energies in kcal/mol for the model reactions discussed in the introduction. Table II gives the vacuum translational, rotational, and vibrational energies and entropies at 298.15 K that are used to calculate the total enthalpy, entropy, and free energy changes from reactant to intermediates and products in Table III and the activation parameters in Table IV. In $(MEHP_T)^-$ (Figure 3b), *all* degrees of freedom are fully optimized, whereas in $(MEHP)^-$ (Figure 3a), H is constrained to O2′ at a distance of 1.96 Å but all other degrees of freedom are optimized. Figure 4 illustrates the *free* energy profile for reaction 2 in vacuum. TS and I denote transition state and intermediate, respectively; the subscript –G or –AC means that the methyl group is oriented –gauche or

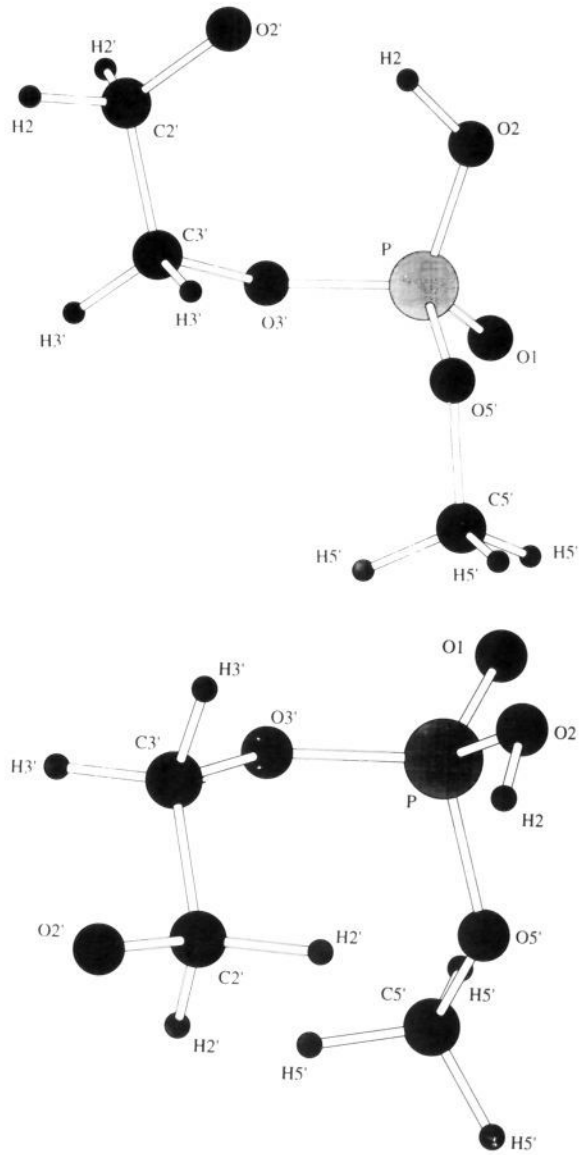

Figure 3. (a) Methyl ethoxy phosphate $(MEHP)^-$ where H is constrained to O2′ at 1.96 Å but all other degrees of freedom optimized. (b) HF/3-21+G* fully optimized methyl ethoxy phosphate $(MEHP_T)^-$.

Table II. HF/3-21+G* Translational, Rotational, and Vibrational Energies and Entropies at 298.15 K[a]

	$(MHEP)^-$	$(MEHP_T)^-$	$(TS_{-G}N)^-$	$(I_{-G}N)^-$	$(TS_{-G}R)^{-}$[b]	$(I_{-G}X)^-$	$(TS_{-AC}X)^-$	$(EP)^-$ + MeOH
E_{trans}	0.889	0.889	0.889	0.889	0.889	0.889	0.889	1.778
E_{rot}	0.889	0.889	0.889	0.889	0.889	0.889	0.889	1.778
E_{vib}	90.404	88.491	88.856	90.057	88.611	90.069	87.459	86.117
E_{total}[c]	92.182	89.268	90.634	91.835	90.389	91.846	89.237	89.672
S_{trans}	41.025	41.025	41.025	41.025	41.025	41.025	41.025	76.659
S_{rot}	29.430	29.753	29.081	28.943	28.956	28.938	29.202	46.332
S_{vib}	27.560	32.946	23.066	22.888	23.176	22.467	26.349	13.892
S_{total}[d]	98.015	103.724	93.172	92.857	93.157	92.429	96.576	136.882

[a] Energies in kcal/mol; entropies in cal/mol/K. [b] Rotational transition state for $(I_{-G}N)^- \rightarrow (I_{-G}X)^-$; $E_{HF} = -829.193\,43$; $E_{MP2} = -834.811\,63$. [c] $E_{total} = E_{trans} + E_{rot} + E_{vib}$. [d] $S_{total} = S_{trans} + S_{rot} + S_{vib}$.

Table III. Free Energy, Enthalpy, and Entropy Changes at 298.15 K[a]

$(MHEP)^- \rightarrow$	$(MEHP)^-$	$(MEHP_T)^-$	$(I_{-G}N)^-$	$(I_{-G}X)^-$	$(EP)^- +$ MeOH
ΔE_{HF}[b]	31.9	50.2	34.5	34.6	27.3
ΔE_{MP2}[b]	33.1	51.2	29.7	29.5	22.3
Δh[c]		-1.9	-0.3	-0.3	-1.9
ΔH[d]		49.3	29.4	29.2	20.4
$T\Delta S$[e]		1.7	-1.5	-1.5	11.6
ΔG[f]		47.6	30.9	30.7	8.8

[a] Energies in kcal/mol and entropies in cal/mol/K; zero of energy equals $(MHEP)^-$ reactant. [b] Energies from Table I. [c] $\Delta h = \Delta E_{total} + P\Delta V$, where $PV = RT = 0.592$ kcal/mol. [d] $\Delta H = \Delta E_{MP2} + \Delta h$. [e] $T\Delta S = \Delta S_{total} * 298.15 \times 10^{-3}$. [f] $\Delta G = \Delta H - T\Delta S$.

–anticlinal with respect to the basal ring oxygen; N and X denote endocyclic and exocyclic cleavage, respectively; R denotes rotation about the P–O(H) bond, and the superscript represents the total charge of the molecule.

Proton transfer from O2′ to O2 in $(MHEP)^-$ can yield either an *acyclic tetravalent* phosphate intermediate $(MEHP_T)^-$ (Figure 3b) or a *cyclic pentacovalent* phosphorane intermediate (Figure 2). The former is stabilized in a conformation where C2′–O2′ is trans to C3′–O3′ (Figure 3b). The latter is found in two conformations; viz., $(I_{-G}N)^-$ in Figure 2a and $(I_{-G}X)^-$ in Figure 2b with the phosphoryl hydrogen roughly 2 Å from the departing oxygen in endocyclic and exocyclic cleavage, respectively. The difference in energy between the $(I_{-G}N)^-$ and $(I_{-G}X)^-$ intermediates is less than 0.2 kcal/mol. Since the *free* energy for the formation of a tetravalent $(MEHP_T)^-$ intermediate from $(MHEP)^-$ is ≈17 kcal/mol greater than that of a pentacovalent $(I_{-G}N)^-$ or $(I_{-G}X)^-$ intermediate (Table III), ring-closure is the lower energy pathway. The formation free energy of both tetravalent and pentavalent intermediates is positive at 298 K and is dominated by the enthalpy change; the magnitude of the entropic effects and the vibrational energy changes are small (≤2 kcal/mol). Electron correlation corrections lower ΔE_{HF} for the formation of the pentacovalent intermediates and the products by ≈5 kcal/mol (Table III). The overall gas-phase reaction, $(MHEP)^- \rightarrow (EP)^- + MeOH$, at 298 K is computed to be thermodynamically unfavorable ($\Delta G = 8.8$ kcal/mol).

Table IV shows that the activation energy $\Delta E_{HF}^{\dagger}$ for $(I_{-G}N)^- \rightarrow (TS_{-G}N)^-$ is less than $\Delta E_{HF}^{\dagger}$ for $(I_{-G}N)^- \rightarrow (TS_{-G}R)^-$ or $\Delta E_{HF}^{\dagger}$ for $(I_{-G}X)^- \rightarrow (TS_{-AC}X)^-$. Comparison of $\Delta E_{HF}^{\dagger}$ with $\Delta E_{MP2}^{\dagger}$ in Table IV shows that the correlation energy corrections are ≤3.6 kcal/mol. The vibrational energy changes ($\Delta h^{\dagger}$ in Table IV) are small, ≤2.6 kcal/mol. The magnitude of the entropic change ($T\Delta S^{\dagger}$) is small (less than 1.4 kcal/mol) except in forming the products, $(EP)^- + MeOH$, where $T\Delta S^{\dagger} = 12$ kcal/mol. The relative free energies in Table IV and Figure 4 show that the rate-limiting step in the overall gas-phase reaction

$$(MHEP)^- \rightleftharpoons (I_{-G}N)^- \rightleftharpoons (I_{-G}X)^- \rightarrow (EP)^- + MeOH$$

is formation of the cyclic phosphate $(EP)^-$.

The Mulliken atomic charges for the acyclic and cyclic structures are given in Table V. Although a Mulliken population analysis is not unique, it is useful for comparing different molecules using the same basis set for each molecule. Table V shows that when the hydrogen is constrained to a phosphoryl oxygen in $(MEHP)^-$, the phosphorus atom is more electropositive (by 0.08), whereas O2′ is more electronegative (by −0.21) relative to $(MHEP)^-$. As a result, the negative charge density is concentrated on O1, O2, and O2′ in $(MEHP)^-$, whereas it is mainly on the phosphoryl oxygens O1 and O2 in $(MHEP)^-$ (see section 4.2). In analogy to $(MEHP)^-$, the phosphorus atom is more electropositive (by 0.11), whereas O2′ is more electronegative (by −0.13) in $(TS_{-G}N)^-$ relative to $(MHEP)^-$. In the transition state for endocyclic or exocyclic cleavage, the basal atoms are less electropositive (P)/electronegative (O1, O2, O3′), whereas the axial atoms are more electronegative (O2′, O5′)/electropositive (H) than the corresponding atoms in the respective intermediate. Although there is greater charge on the departing apical oxygen relative to the other apical oxygen or basal ring oxygen in the trigonal-bipyramidal transition state and intermediate for exocyclic or endocyclic cleavage, the maximum electron density is not located on the departing oxygen but is concentrated on the phosphoryl oxygens (O1 and/or O2).

The ab initio results indicate that the gas-phase reaction 2 proceeds via a stepwise mechanism involving a monoanionic *pentacovalent* phosphorane intermediate, $(I_{-G}N)^-$, with the phosphoryl hydrogen ≈2 Å from the departing ring oxygen (O2′) for endocyclic cleavage. The phosphoryl hydrogen then rotates to within 2 Å of the departing methoxy oxygen (O5′) to yield an intermediate $(I_{-G}X)^-$ which undergoes rate-limiting exocyclic cleavage. Solvent effects do not alter the gas-phase reaction profile qualitatively; i.e., as in vacuum, the solution free energy barrier for exocyclic cleavage is more than twice that for endocyclic cleavage.[20] The stereochemistry of the reaction in Figure 4 is in accord with axial attack and axial departure; i.e., an in-line mechanism. Pseudorotation of $(I_{-G}N)^-$ or $(I_{-G}X)^-$ to yield an intermediate with the methyl group equatorial and the hydroxyl group axial is computed to be energetically unfavorable,[20] thus

Table IV. Activation Parameters at 298.15 K[a]

ground state / transition state	$(MHEP)^-$ / $(TS_{-G}N)^-$	$(I_{-G}N)^-$ / $(TS_{-G}N)^-$	$(I_{-G}N)^-$ / $(TS_{-G}R)^-$	$(I_{-G}X)^-$ / $(TS_{-AC}X)^-$	$(EP)^- +$ MeOH / $(TS_{-AC}X)^-$
$\Delta E_{HF}^{\dagger}$[b]	38.6	4.2	11.2	17.2	24.6
$\Delta E_{MP2}^{\dagger}$[b]	35.5	5.8	10.5	13.7	21.0
$\Delta h^{\dagger}$[c]	-1.5	-1.2	-1.4	-2.6	-1.0
$\Delta H^{\dagger}$[d]	34.0	4.6	9.1	11.1	20.0
$T\Delta S^{\dagger}$[e]	-1.4	0.1	0.1	1.2	-12.0
$\Delta G^{\dagger}$[f]	35.4	4.5	9.0	9.9	32.0

[a] Energies in kcal/mol and entropies in cal/mol/K relative to ground state. [b] Energies from Table I and Table II. [c] $\Delta h^{\dagger} = \Delta E_{total} + P\Delta V$, where $PV = RT = 0.592$ kcal/mol. [d] $\Delta H^{\dagger} = \Delta E_{MP2}^{\dagger} + \Delta h^{\dagger}$. [e] $T\Delta S^{\dagger} = \Delta S_{total} * 298.15 \times 10^{-3}$. [f] $\Delta G^{\dagger} = \Delta H^{\dagger} - T\Delta S^{\dagger}$.

Table V. HF/3-21+G* Mulliken Atomic Charges

	$(MHEP)^-$	$(MEHP)^-$[a]	$(TS_{-G}N)^-$	$(I_{-G}N)^-$	$(TS_{-G}R)^-$	$(I_{-G}X)^-$	$(TS_{-AC}X)^-$
Q(P)	2.04	2.12	2.15	2.21	2.11	2.21	2.08
Q(O1)	-0.90	-0.86	-0.86	-0.99	-1.03	-0.99	-0.81
Q(O2)	-0.99	-0.89	-0.89	-0.90	-0.92	-0.90	-0.86
Q(O3′)	-0.55	-0.54	-0.52	-0.53	-0.51	-0.52	-0.39
Q(O2′)	-0.66	-0.87	-0.79	-0.63	-0.48	-0.52	-0.53
Q(O5′)	-0.54	-0.52	-0.49	-0.46	-0.41	-0.57	-0.78
Q(H)	0.56	0.58	0.57	0.52	0.47	0.52	0.58
Q(C3′)[b]	0.15	0.14	-0.23	-0.27	-0.26	-0.26	-0.15
Q(C2′)[b]	-0.08	-0.14	-0.11	0.12	0.12	0.12	-0.02
Q(C5′)[b]	-0.04	-0.01	-0.05	-0.07	-0.08	-0.09	-0.10

[a] Stationary point for H–O2′ fixed at 1.96 Å. [b] Charges for extended carbon atoms.

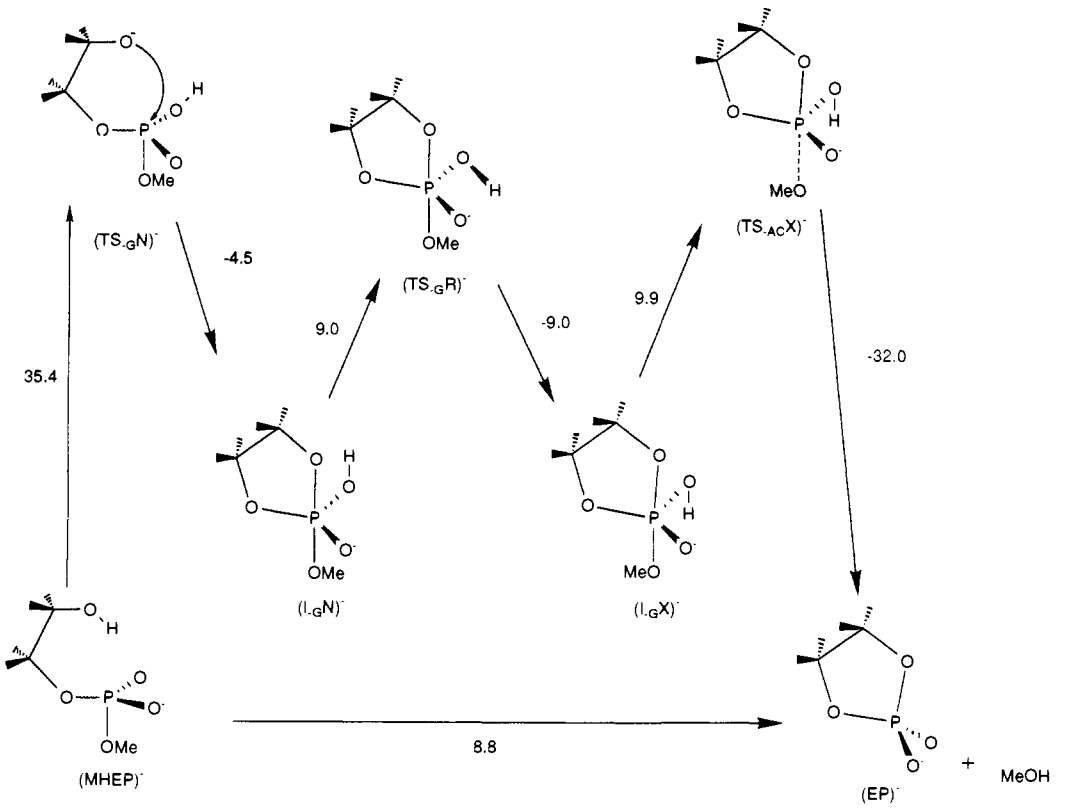

Figure 4. Free energy gas-phase profile for $(MHEP)^- \rightarrow (EP)^- + (OH)^-$. All structures are fully optimized at the HF/3-21+G* level. The numbers are gas-phase free energies in kcal/mole from Tables III and IV.

eliminating the possibility of an adjacent mechanism for reaction 2.

4. Discussion

In the following, the results in section 3 are compared to 3-21+G* results for the base-catalyzed hydrolysis of ethylene phosphate,[13,12] a model for the RNase A-catalyzed hydrolysis of ribonucleic acids. On the basis of the present calculations and previous ab initio[13,12] and simulation results,[11,21] a new mechanism for the RNase A-catalyzed cyclization step is proposed. This mechanism is compared to the standard and Breslow's mechanism (see Introduction) as well as to the nonenzymatic reaction in solution.

4.1. Comparison with Dianionic Intermediates. The approach of two negative ions, $(OH)^-$ and $(EP)^-$, in the gas phase has been computed at the 3-21+G* level to result in *ring-opening* and formation of a *dianionic tetravalent* phosphate intermediate.[13,12] In contrast, the attack of neutral MeOH on $(EP)^-$ anion in the gas phase (reverse of reaction 2, Figure 4) results in *ring-closure* and formation of a *monoanionic pentacovalent* phosphorane intermediate, instead of a tetravalent phosphate $(MEHP_T)^-$ intermediate (Figure 3b) which is higher in energy (see Table I). For both monoanionic and dianionic[12-15] transition states, a distorted trigonal-bipyramidal geometry is found, and the location of the transition state is similar (at a reaction coordinate around 2.3 ± 0.2 Å). The $(TS_{-G}N)^-$ and $(TS_{-AC}X)^-$ transition states appear to be stereoelectronically favorable; i.e., the hydroxy hydrogen is oriented such that the phosphoryl oxygen O2 has a lone pair that is antiperiplanar to the breaking bond, which may exist endocyclic or exocyclic cleavage. Equatorial P–O2(H) bond rotation of $(I_{-G}N)^-$ to yield $(I_{-G}X)^-$ is required for the computed in-line mechanism. This is in accord with ab initio results for the base-catalyzed methanolysis[15] and hydrolysis[14] of dimethyl phosphate where the lowest energy pathway was determined by rotation about an equatorial P–O bond during the reaction to yield stereoelectronically favorable transition states.

(20) Lim, C.; Tole, P. *J. Phys. Chem.* **1992**, *96*, 5217-5218.

4.2. Relevance to RNase A-Catalyzed Transphosphorylation. Figure 5 illustrates the proposed mechanism for the RNase A-catalyzed transphosphorylation step; for clarity, only the key interactions of the active site residues, His 12, Lys 41, and His 119, with the substrate are shown. The average molecular dynamics structure of RNase A/CpA with His 12 neutral shows that Lys 41 hydrogen bonds to O2′, His 12 to the sugar hydroxyl hydrogen, and His 119 to a phosphoryl oxygen;[11] these interactions are depicted in **1**, Figure 5. His 12 is in a position to facilitate rapid tautomeric conversion to **3** via **2**; this is in accord with kinetic studies by T-jump chemical relaxation of prototropic tautomeric equilibria which show that a dissociative acid/base-catalyzed mechanism dominates the kinetics of tautomerization.[22] The resulting tautomer **3** may be stabilized by active site interactions, as suggested by molecular dynamics simulations of RNase A complexed to a substrate analogue, deoxy-CpA,[23] a substrate, CpA,[11] and a product, 3′-UMP.[21] The average molecular dynamics structures of these RNase A complexes with His 12 neutral and positively charged (His 119 is protonated in all the structures) show that Lys 41 hydrogen bonds to O2′ (except in the deoxy-CpA structures and the CpA complex with His 12 protonated), His 12 hydrogen bonds to O2′ and/or a phosphoryl oxygen, and His 119 hydrogen bonds to a phosphoryl oxygen. Thus the negative charge density in **3**, which is concentrated on O1, O2, and O2′ (see section 3 and Table V), can be partially neutralized by interactions with the side chain of His 119, His 12, and Lys 41, respectively. Although the proton from Lys 41 can transfer to O2′, this may not occur since Lys 41 hydrogen bonds to other residues (Asn 44 and Gln 11) and water molecules in the average molecular dynamics structure of the RNase A/CpA complex with His 12 neutral. Water molecules and other residues, e.g., Phe 120 and/or Gln 11, can also hydrogen bond to the phosphoryl oxygens and stabilize **3**. Similar interactions may exist to stabilize the endocyclic cleavage transition state **4**; i.e., Lys 41 hydrogen bonds to O2′, whereas His 12, His 119, Phe 120, Gln, 11, and water molecules interact with the phosphoryl oxygens. These interactions were found in the neutron/X-ray structure of RNase A complexed to a transition state analogue, uridine vanadate (UVC).[24]

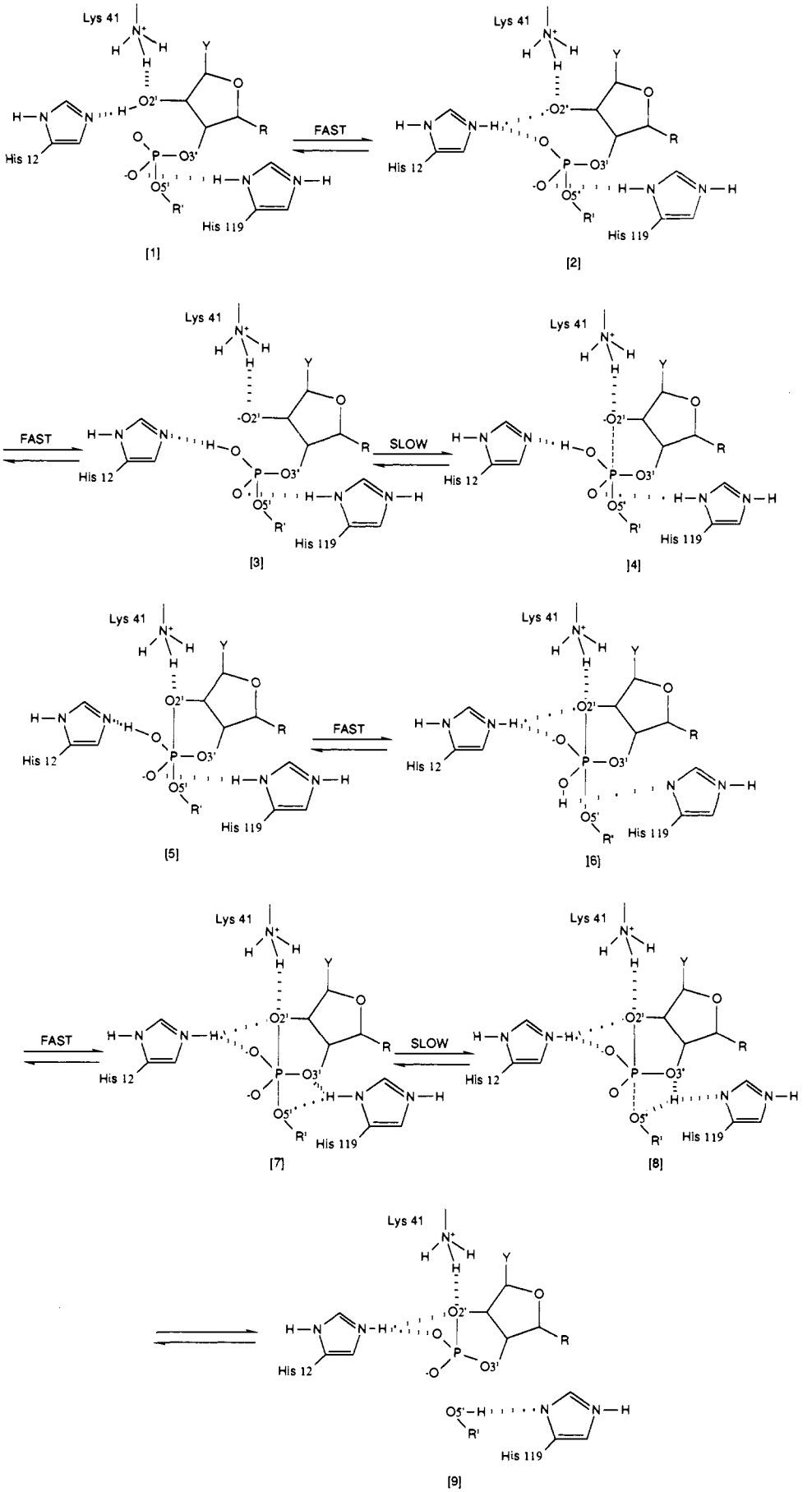

Figure 5. A schematic representation of the proposed mechanism for RNase A-catalyzed transphosphorylation step. For clarity, the key interactions of the active site residues, His 12, Lys 41, and His 119, with the substrate are shown; interactions of other residues, e.g., Phe 120 and Gln 11, and water molecules with the substrate are also likely (see text) but are not shown.

The average molecular dynamics structure of the RNase A/CpA complex with *His 12 and His 119 positively charged* shows that both histidines hydrogen bond to a phosphoryl oxygen (O1 or O2) but His 12 is located near the cytidine side (NE2 of His 12 is 3.4, 2.9, 3.3, and 4.8 Å from O1, O2, O2′(cytidine), and O5′(adenosine), respectively), whereas His 119 is positioned near the adenosine side (ND1 of His 119 is 2.8, 4.7, 4.1, and 3.6 Å from O1, O2, O2′(cytidine), and O5′(adenosine), respectively). The two active site histidines are thus in a position to facilitate the conformational change required for exocyclic cleavage since His 12 can remove the phosphoryl hydrogen, while His 119 protonates a phosphoryl oxygen to yield the conformation in **6**; this illustrates how the significant gas-phase rotational barrier for $(I_{-G}N)^- \rightarrow (TS_{-G}R)^- \rightarrow (I_{-G}X)^-$ in Figure 4 may be lowered in His 12 and His 119 and the importance of their location in the active site. The stereochemistry of the proposed mechanism in Figure 5 is thus consistent with an in-line mechanism found by Usher et al.[25] His 119 can catalyze formation of the cyclic phosphate intermediate by facilitating the transfer of the proton (which it had originally donated) from the intermediate **6** to the leaving O5′ group; in this way, His 119 can stabilize the developing charge on O5′ in the exocyclic cleavage transition state **8**. The latter can be further stabilized by active site interactions similar to those in the endocyclic cleavage transition state **4**. In particular, the phosphoryl oxygens, which have the most negative charge (see section 3 and Table V), in the exocyclic cleavage transition state **8** and cyclic phosphate can be stabilized by hydrogen bonds from protonated His 12, Phe 120 and/or Gln 11 as well as water molecules. These interactions were found in the X-ray structures of RNase A complexed to the UVC transition state analogue[24] and cyclic cytidine monophosphate.[11]

Prototropic tautomeric equilibrium generally occurs rapidly (half-life below a few milliseconds);[22] i.e., **1** ⇌ **2**, **2** ⇌ **3**, **5** ⇌ **6**, and **6** ⇌ **7** are fast relative to **3** → **4** or **6** → **8**. Thus, His 12 catalyzes formation of **3** which is activated for formation of phosphorane monoanion **5** since the phosphorus atom is more electropositive and O2′$^-$ is more electronegative in **3** compared to the corresponding atoms in **1** (see section 3 and Table V with $(MEHP)^-$ and $(MHEP)^-$ modelling **3** and **1**, respectively). The active site residues, His 12, His 119, Lys 41, Phe 120, and/or Gln 11, and water molecules help to stabilize both **3** and **4**. This causes ground-state destabilization and transition state stabilization so that the activation energy for phosphorane intermediate formation is lower in the enzyme relative to vacuum. His 119 catalyzes the formation of the cyclic phosphate intermediate by stabilizing the developing charge on O5′ in **8**, whereas His 12, Lys 41, Gln 11, Phe 120, and water molecules help to stabilize the negative charge on the phosphoryl and ring oxygens in **8**, thus stabilizing the exocyclic cleavage transition state.

4.3. Comparison with Other Enzymatic Transphosphorylation Mechanisms and Corresponding Nonenzymatic Reaction in Solution. A key difference between the proposed mechanism in Figure 5 and the standard mechanism (concerted general acid–base catalysis)[3] is that a *negatively charged* O2′ attacks a *monoanionic* phosphate **2** in the latter but a *neutral* phosphate **3** in the former. Ab initio calculations of the $(EP)^- + (OH)^-$ system[12] show that $(OH)^-$ attack on ethylene phosphate is concerted with ring opening. Stated alternatively, ring-closure of the *dianionic* tetrahedral intermediate $^-OCH_2CH_2PO_4H^-$, is concerted with $(OH)^-$ elimination; this can be used to model concerted general acid–base catalysis in the standard mechanism which assumes that a single dianionic transition state is involved. The $\Delta E_{MP2}^{\dagger}$ barrier is 48 kcal/mol for ring-closure of the dianionic tetrahedral phosphate, modelling O2′$^-$ attack on the monoanionic phosphate in **2**. Modelling step **3** → **4** in the proposed mechanism by $(MEHP)^- \rightarrow (TS_{-G}N)^-$, the $\Delta E_{MP2}^{\dagger}$ barrier is only 2.4 kcal/mol (see Table I). Thus, attack of a *negatively charged* O2′ on a *monoanionic* phosphate **2** requires much more energy than O2′$^-$ attack on a *neutral* phosphate **3**. The gas-phase activation free energy (Table IV and Figure 4) for $(I_{-G}N)^- \rightarrow (I_{-G}X)^-$ (9 kcal/mol), modelling **5** → **6**, or for $(I_{-G}X)^- \rightarrow (EP)^- + MeOH$ (10 kcal/mol), modelling **6** → **9**, is less than that for ring-closure of the dianionic tetrahedral phosphate (48 kcal/mol).[12] This difference is not altered by solvation effects; i.e., the *solution* activation free energy[20,26] for $(MEHP)^- \rightarrow (TS_{-G}N)^-$, or $(I_{-G}N)^- \rightarrow (TS_{-G}R)^-$, or $(I_{-G}X)^- \rightarrow (TS_{-AC}X)^-$, is also much less than that for ring-closure of the *dianionic* tetrahedral phosphate.[12] Thus the barrier involved in the standard mechanism is probably greater than any of the barriers in the proposed mechanism indicating that the latter proceeds via a lower energy pathway than the standard one.

The average molecular dynamics structure of the RNase A/CpA complex with His 12 *neutral* and His 119 positively charged shows that NE2 of His 12 is 3.0, 3.4, 4.0, and 5.5 Å from O2′(cytidine), O2, O1, and O5′(adenosine), respectively, whereas ND1 of His 119 is 6.0, 4.8, 2.4, and 3.6 Å from O2′(cytidine), O2, O1, and O5′(adenosine), respectively. Since NE2 of His 12 is within 3.5 Å of O2′ and O2, His 12-catalyzed proton transfer from O2′ to a phosphoryl oxygen will result in formation of the endocyclic cleavage intermediate **5** where the phosphoryl hydrogen is closer to "endocyclic" O2′ than to O5′. In contrast, ND1 of His 119 is closer to O1 and O5′ than to O2 and O2′. Protonation of the phosphate monoanion by His 119 and deprotonation of the 2′-hydroxyl group by His 12, as in Breslow's mechanism, will result in formation of the exocyclic cleavage intermediate **6** where the phosphoryl hydrogen is closer to "exocyclic" O5′ than to O2′. Thus the difference between the proposed mechanism and Breslow's is that the latter results in an exocyclic cleavage intermediate **6** instead of an endocyclic cleavage intermediate **5**. The ab initio calculations[26] show that ring-opening of $(I_{-G}X)^-$, modelling **6**, requires far greater energy than endocyclic cleavage of $(I_{-G}N)^-$, modelling **5**. This implies that in Breslow's mechanism, the transition state involved in phosphorane monoanion formation is higher in energy than the corresponding transition state **4** in the proposed mechanism.

In the absence of RNase A, the tautomer **3** will be destabilized and the tautomeric equilibrium is greatly shifted to **1**, in accord with the solution pK_a values of phosphate and alcohol groups (see Introduction); i.e., the ratio of **1** to **3** in solution is roughly of the order of 10^{12}. Furthermore, without the stabilizing interactions of the active site residues, the transition state **4** will be destabilized. Thus, relative to the enzyme, the ground state in solution is stabilized, whereas the solution transition state is destabilized, hence the activation energy for formation of phosphorane intermediate **5** in solution is greater than that in the enzyme. Without the precise positioning of His 12 and His 119 catalyzing the tautomeric conversion from **5** to **6**, the rotational barrier for **5** → **6** in solution is expected to be greater than that in the enzyme. In the absence of stabilizing active site interactions, the transition state **8** will be destabilized in solution relative to the enzyme so that the activation energy for cyclic phosphate formation in solution is greater than that in the enzyme.

5. Concluding Discussion

Using ab initio molecular orbital calculations, we have mapped out the free energy profile for reaction 2 (Figure 4), a model for the transphosphorylation step in RNase A catalysis. The gas-phase reaction 2 proceeds via a stepwise mechanism involving monoanionic *pentacovalent* intermediates, $(I_{-G}N)^-$ and $(I_{-G}X)^-$. Rotation about the equatorial P–O2 bond of $(I_{-G}N)^-$ to yield $(I_{-G}X)^-$ is required for rate-limiting exocyclic cleavage and an in-line mechanism. The pentacovalent intermediates and transition states have a distorted trigonal-bipyramidal geometry, and the

(21) Straub, J.; Lim, C.; Karplus, M., submitted for publication.
(22) Dubois, J. E.; Drefus, M. Dynamic Study by Chemical Relaxation of Prototropic Equilibria in Solution: Recent Advances. In *Protons and Ions Involved in Fast Dynamic Phenomena*; Laszlo, P., Ed.; Elsevier: 1977; p 169.
(23) Lim, C.; Karplus, M., unpublished results.
(24) Wlodawer, A.; Borkakoti, N.; Moss, D. S.; Howlin, B. *Acta Crystallogr.* **1986**, *B42*, 379–387.
(25) Usher, D. A.; Erenrich, E. S.; Eckstein, F. *Proc. Natl. Acad. Sci. U.S.A.* **1972**, *69*, 115–118.
(26) Tole, P.; Lim, C., manuscript in preparation.

conformation of the transition states is activated for endocyclic and exocyclic cleavage. Pseudorotation of $(I_GN)^-$ or $(I_GX)^-$ to an intermediate with the methyl group equatorial and the hydroxyl group axial is energetically unfavorable.[20] Solvent effects do not alter the gas-phase reaction profile qualitatively since the solution free energy barrier for exocyclic cleavage is more than twice that for endocyclic cleavage, as in vacuum.[20]

The present and previous ab initio calculations in conjunction with molecular dynamics simulations of the RNase A complexes[11,21] and experimental data suggest a more detailed mechanism for the RNase A-catalyzed transphosphorylation step; this is summarized in Figure 5. In particular, the proposed mechanism shows that the precise alignment of three key active site residues; viz., His 12, His 119, and Lys 41, is crucial in determining the lowest energy pathway for the transphosphorylation step. His 12 is positioned to facilitate the transfer of the proton on O2′ in **1** to a phosphoryl oxygen to yield **3**. Lys 41 is in a position to stabilize **3** and the endocyclic cleavage transition state **4**; both **3** and **4** can be also be stabilized by active site residues (His 12, His 119, Phe 120, and/or Gln 11) and water molecules so that the barrier to phosphorane monoanion intermediate formation is reduced relative to vacuum or solution. The two active site histidines are positioned so that His 12 can remove the phosphoryl hydrogen in **5**, while His 119 protonates the phosphoryl oxygen to yield **6**, whose conformation is activated for exocyclic cleavage. His 119 is positioned to facilitate the transfer of the proton on a phosphoryl oxygen in **6** to O5′, thus stabilizing the developing charge on O5′ in the exocyclic cleavage transition state **8**; the phosphoryl and ring oxygens in **8** can be stabilized by interactions from His 12, Lys 41, Phe 120, and/or Gln 11 and water molecules. The stereochemistry of the proposed mechanism for transphosphorylation in RNase A catalysis is in-line, as observed experimentally.

Acknowledgment. We thank Professor Ronald Kluger, Professor Jik Chin, and Dr. Krishnan Raghavachari for stimulating discussions. The calculations were performed using GAUSSIAN 90 on a Stardent PS3030 and on a Cray XMP at the Ontario Center for Large Scale Computation.

Registry No. RNase, 9001-99-4.

Localization Properties of π Electrons and the Validity of Independent-Particle Models for Hydrocarbon Compounds

Johannes Schütt and Michael C. Böhm*

Contribution from the Institut für Physikalische Chemie, Physikalische Chemie III, Technische Hochschule Darmstadt, D-6100 Darmstadt, Federal Republic of Germany.
Received January 13, 1992

Abstract: The electronic localization properties in alternant and nonalternant hydrocarbon π compounds are quantified in terms of the mean-square deviation of the π electron density $\langle(\Delta n_i^2)\rangle$ around the corresponding mean value $\langle n_i\rangle$. To derive the correlated ground state, the method of the local approach (LA) is employed. The computational method for the π subspace is a simple Hückel-type operator for the one-determinantal wave function and a model Hamiltonian defined by Hartree–Fock hopping terms to evaluate the correlated ground state. The integrals are calculated ab initio in a single-ζ Slater-type basis. The π electrons in hydrocarbons are sizeably localized. This also holds for extended polyenes and $4n + 2$ monocycles. In addition to the electronic charge fluctuations $\langle(\Delta n_i^2)\rangle$, two atomic electron density localization parameters Δ_i and Σ_i are defined to analyze the π electron localization and the importance of the electron–electron interaction in π bonds. The respective atomic electron density localization depends on the topology of the selected "reference center". Bond length alternation leads to an enhancement of the π electronic charge fluctuations, i.e., they are better delocalized here. Interatomic sharing is enlarged. The latter enhancement accompanying bond alternation increases with enlarged electron–electron interaction. Bond length alternation and the uneven charge distribution in certain nonalternant hydrocarbons support the π electron delocalization in the respective networks. On the basis of the calculated π electron localization parameters Δ_i an instability index γ_{in} for nonalternant π systems is suggested. Calculated γ_{in} elements agree well with the known experimental status of the considered π systems. An analysis of the π correlation energy is given for polyenes and monocyclic annulenes as a function of the bond alternation. The competition between π and σ correlation effects is studied by a semiempirical INDO (intermediate neglect of differential overlap) model.

1. Introduction

The electronic structure properties of hydrocarbon π systems have absorbed the interest of theoretical chemists and physicists for more than 60 years. For a very long time it has been assumed throughout in the chemical community that π electrons, especially those in extended networks, are close to the free-electron behavior and highly delocalized. It has been and it is still common usage to characterize molecular geometries without bond length alternation as "delocalized" structures, while bondlength alternation universally is equated with "localized π electron systems". In this context it is remarkable that the two labels "delocalized versus localized π electron systems" have their roots in a purely descriptive language, but not in unambiguously defined quantum chemical expectation values. Only the following two statements can be extracted from static electron density distributions. Molecular structures without bond alternation indicate in the first place an even electron distribution. Spatial differences in the density distribution are present in structures with bond alternation. This and only this follows from molecular geometries and the associated electron density. Any argumentation beyond the latter statements, e.g., the widely assumed 1:1 correspondence between bond alternation and electronic localization, cannot be justified a priori as it violates a fundamental principle of quantum mechanics, i.e., the indistinguishability of electrons. The bottleneck in the above widely used interpretation will be explained in the present investigation intended to introduce a well-defined localization measure for electrons in chemical bonds.

The frequent adoption of free-electron approaches together with the use of descriptive labels for the interpretation of π electron properties had been possible in the past due to the remarkable success of simple one-electron theories. By using the well-known Hückel molecular orbital (HMO) model[1] or the free-electron (FE)

(1) Hückel, E. Z. *Physik* **1931**, *70*, 204; **1932**, *76*, 68.

0002-7863/92/1514-7252$03.00/0